

UltraVSR: Achieving Ultra-Realistic Video Super-Resolution with Efficient One-Step Diffusion Space

Yong Liu^{1,2}, Jinshan Pan³, Yinchuan Li⁴, Qingji Dong^{1,2}, Chao Zhu^{1,2}, Yu Guo^{1,2}, Fei Wang^{1,2,†}

¹ National Key Laboratory of Human-Machine Hybrid Augmented Intelligence

² IAIR, Xi'an Jiaotong University ³ Nanjing University of Science and Technology ⁴ Huawei Noah's Ark Lab
liuy1996v@qq.com, wfx@xjtu.edu.cn

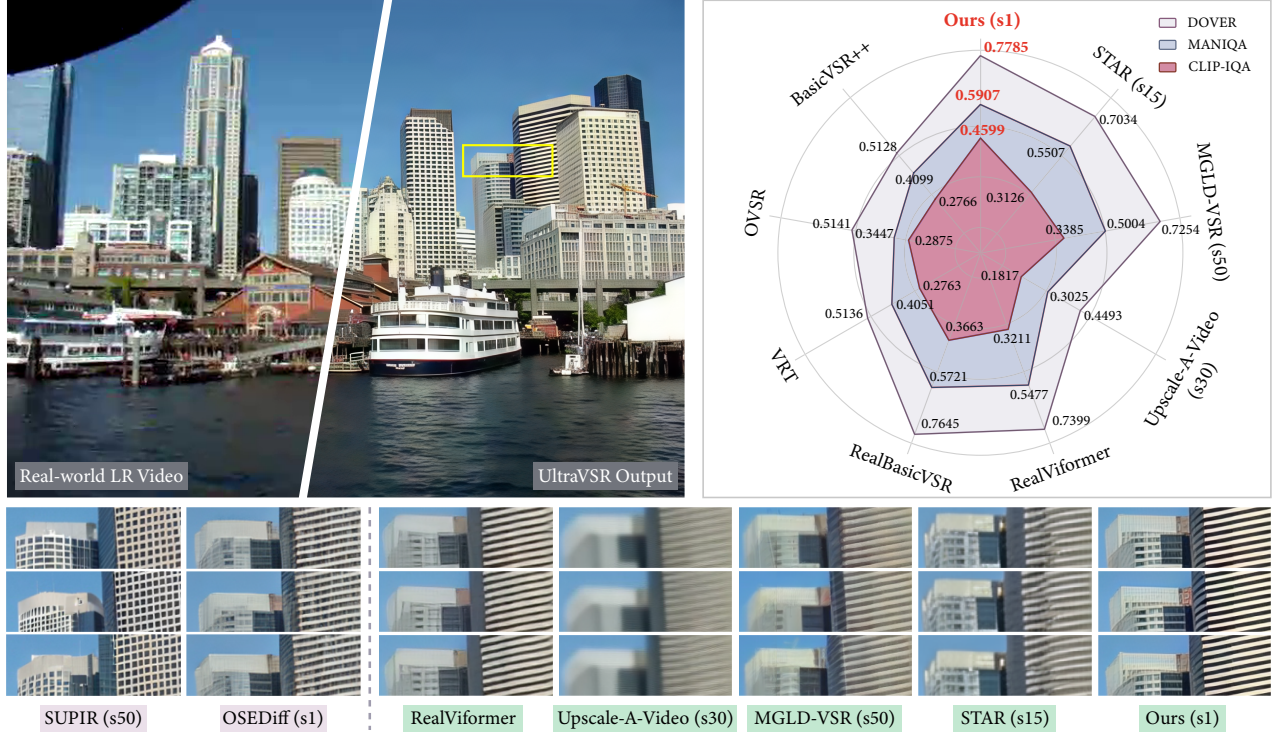


Figure 1: Quantitative and qualitative VSR comparisons. Top-left: An example on a real-world low-resolution (LR) video frame; Top-right: Quantitative comparison with state-of-the-art VSR approaches on the VideoLQ benchmark [7], where our approach achieves leading scores across all three metrics with just a one-step (s1) sampling process; Bottom: Visual comparison across three consecutive frames. SISr approaches often suffer from temporal inconsistency, while VSR approaches typically lack fine texture details. In contrast, our approach produces visually realistic and temporally coherent results.

ABSTRACT

Diffusion models have shown great potential in generating realistic image detail. However, adapting these models to video super-resolution (VSR) remains challenging due to their inherent stochasticity and lack of temporal modeling, which together hinder the preservation of temporal consistency across frames. Previous methods have attempted to mitigate this issue by incorporating motion information and temporal layers. However, motion estimation from low-resolution videos is often unreliable due to missing fine details. Furthermore, these approaches typically rely on deep temporal layers and require multiple sampling steps per frame, resulting in high computational costs and limiting their applicability to short video sequences. In this paper, we propose UltraVSR, a novel framework that enables ultra-realistic and temporal-coherent VSR through an

efficient one-step diffusion space. A central component of UltraVSR is the Degradation-aware Restoration Schedule (DRS), which estimates a degradation factor from the low-resolution input and transforms iterative denoising process into a single-step reconstruction from low-resolution to high-resolution videos. This design eliminates randomness from diffusion noise and significantly speeds up inference. To ensure temporal consistency, we propose a lightweight yet effective Recurrent Temporal Shift (RTS) module, composed of an RTS-convolution unit and an RTS-attention unit. By partially shifting feature components along the temporal dimension, these two units collaboratively facilitate effective feature propagation, fusion, and alignment across neighboring frames, without relying on explicit temporal layers. The RTS module is integrated into a pretrained text-to-image diffusion model and is further enhanced through Spatio-temporal Joint Distillation (SJD), which

improves temporal coherence while preserving realistic details. Additionally, we introduce a Temporally Asynchronous Inference (TAI) strategy to capture long-range temporal dependencies under limited memory constraints. Extensive experiments show that UltraVSR achieves state-of-the-art performance, both qualitatively and quantitatively, in a single sampling step.

CCS CONCEPTS

• **Computing methodologies** → **Reconstruction**; *Image processing*; Computational photography.

KEYWORDS

Video super-resolution, Diffusion model, Temporal consistency

1 INTRODUCTION

Video super-resolution (VSR) aims to reconstruct high-resolution (HR) videos from low-resolution (LR) inputs, a task that has garnered significant attention in multimedia and computer vision communities. Unlike single-image super-resolution (SISR), VSR presents additional challenges due to the necessity of maintaining temporal consistency across frames while recovering high-frequency details. With the rapid advancement of deep learning, numerous VSR approaches [1, 5, 6, 10, 13, 16, 22, 47] have emerged over the past decade. However, despite notable progress, existing methods still struggle to restore realistic textures under complex and unknown real-world degradations.

Diffusion models [14, 34] have achieved remarkable success in image synthesis [8, 32], image editing [18, 51] and SISR [39, 43]. However, adapting these diffusion models to VSR remains challenging due to the lack of temporal modeling capabilities. Additionally, the inherent randomness of the diffusion process further exacerbates temporal artifacts such as flickering across frames, e.g., the results of SUPIR [57] and OSedDiff [46] in Fig. 1. Recent approaches, such as MGLD-VSR [53] and Upscale-A-Video [62], attempted to improve temporal consistency by integrating 3D convolutions, temporal attention mechanisms, and motion propagation modules into image diffusion models. Alternatively, text-to-video diffusion models have also been explored for VSR [49]. Nevertheless, these approaches suffer from high computational costs due to the use of temporal layers and unreliable motion information estimated from LR videos. Moreover, these approaches require a large number of sampling steps for each frame, making inference inefficient and impractical, especially for memory-constrained processing of high-resolution and long-duration video sequences.

This paper proposes UltraVSR, an efficient one-step diffusion model for real-world VSR. In contrast to multi-step VSR approaches, UltraVSR introduces a Degradation-aware Restoration Scheduling (DRS) that reformulates the conventional multi-step iterative denoising paradigm as a single-step reconstruction process. DRS first estimates a degradation factor from the input LR video and then maps it with the diffusion noise schedule, thereby achieving single-step reconstruction from LR input to HR video. This scheme eliminates the randomness in the diffusion and significantly improves computational efficiency. To maintain temporal consistency across frames, we develop a lightweight yet effective Recurrent Temporal

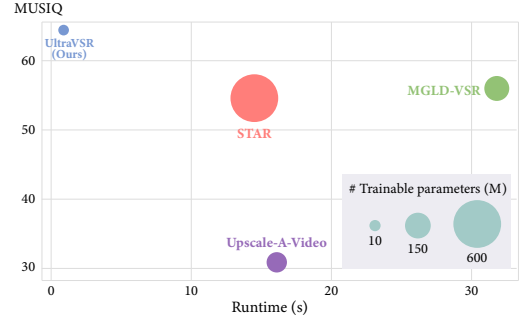


Figure 2: Comparison of runtime and metrics between diffusion-based VSR approaches. Note that the runtime is measured with the HR sequence upscaled to 720×1280. Our approach achieves the fastest speed with better quality.

Shift (RTS) module without explicit temporal layers. The RTS module enables efficient inter-frame feature propagation, fusion, and alignment through two novel units: (1) RTS-convolution unit, which partitions feature maps by channels and shifts groups temporally across adjacent frames for localized feature alignment using 2D convolution; (2) RTS-attention unit, which incorporates temporal shifting operations on *Key/Value* tensors prior to self-attention computation, allowing the model to capture global contextual dependencies.

During training, the RTS module is embedded into a pretrained text-to-image diffusion model and subsequently optimized through Spatio-temporal Joint Distillation (SJD). SJD introduces dual temporal regularizers to separately model real and synthetic video distributions. By minimizing both spatial and temporal gradient discrepancies between two distributions, SJD effectively guides the one-step reconstruction process toward producing visually realistic and temporally consistent HR videos. At inference, we further propose a memory-efficient Temporally Asynchronous Inference (TAI) strategy that decouples spatial and temporal processing by segmenting long video sequences into mini-batches, which are processed independently and then merged prior to RTS propagation. In this way, TAI significantly reduces memory overhead while enabling the model to capture long-range temporal dependencies. Experiments demonstrate that UltraVSR achieves better performance with significantly faster inference, as shown in Fig. 1 and Fig. 2.

In summary, the main contributions of this paper are as follows:

- We propose UltraVSR, an efficient one-step diffusion framework by introducing a Degradation-aware Restoration Scheduling (DRS) for high-quality video reconstruction. To the best of our knowledge, this is the first work to tackle the VSR problem in just one sampling step.
- We develop a lightweight Recurrent Temporal Shift (RTS) that enables effective feature propagation, fusion, and alignment across frames by partially shifting feature components temporally, without relying on explicit temporal layers.
- We introduce Spatio-temporal Joint Distillation (SJD) to enhance temporal coherence and content realism, and propose Temporally Asynchronous Inference (TAI) for memory-efficient long-range dependency modeling.
- Extensive experiments demonstrate that UltraVSR outperforms state-of-the-art methods in both visual quality and

†Corresponding author.

temporal consistency, while significantly accelerating inference speed.

2 RELATED WORK

2.1 Real-World VSR

Numerous VSR methods [5, 10, 13, 22, 23, 25, 48] have been developed to enhance video quality under real-world degradation. For instance, Chan *et al.* proposed RealBasicVSR [7], which removes degradations in videos by introducing a pre-cleaning module and a stochastic degradation scheme. More recently, Zhang *et al.* introduced a channel-attention-based recurrent model, RealViformer [60], based on findings from investigating channel and spatial attention in a real-world setting. Despite these advancements, many approaches remain sensitive to complex, unknown degradations due to limited modeling capacity, leading to inadequate texture recovery and poor generalization.

2.2 Diffusion Model-based VSR

Diffusion models [14, 34] have demonstrated strong performance in generating realistic details for SISR [40, 41, 43, 46, 58]. For example, Yu *et al.* [57] propose SUPIR that expands the scope of image restoration by enhancing perceptual quality and enabling controlled generation via textual prompts, while Wu *et al.* [46] introduce OSediff, an efficient one-step super-resolution method based on variational score distillation [44, 56]. Nevertheless, it is still a non-trivial challenge to scale up these models on VSR task due to the inherent randomness. Recent studies have attempted to address this issue in two ways. On one hand, Zhou *et al.* [62] and Yang *et al.* [53] leverage image diffusion models and propose Upscale-A-Video and MGLD-VSR, respectively, by incorporating additional temporal layers and motion cues extracted from low-resolution (LR) videos. On the other hand, Xie *et al.* [49] build upon a pretrained text-to-video diffusion model and introduce STAR, which employs ControlNet [59] to inject LR video information into the generation process. However, these approaches often rely on multiple sampling steps and complex temporal layers, resulting in high inference latency. To overcome these challenges, we propose an efficient one-step diffusion model for VSR.

3 PROPOSED METHOD

3.1 Overview

Our UltraVSR is built upon the pretrained Stable Diffusion model [32], comprising a VAE encoder/decoder, a text encoder, and a diffusion UNet, as illustrated in Fig. 3. To construct an efficient one-step reconstruction model G_θ to generate HR video V_{HR} from LR input V_{LR} , we introduce three key components: (i) Degradation-aware Reconstruction Scheduling (DRS): Defines a one-step reconstruction from LR videos to HR videos (Sec. 3.2); (ii) Recurrent Temporal Shift (RTS) Module: Incorporates temporal dependencies into the diffusion model by shifting specific feature components across frames, without relying on explicit temporal layers (Sec. 3.3); (iii) Spatio-temporal Joint Distillation (SJD): Guides training with the content realistic and temporal coherent supervision (Sec. 3.4).

Given an input LR video sequence V_{LR} , UltraVSR first estimates a degradation factor d and determines a corresponding reconstruction time step t_{rec} . Concurrently, a text prompt is simultaneously extracted from V_{LR} via the text encoder, while a latent representation z_{LR} is derived using the VAE encoder. These variables are fed into the diffusion UNet together to produce intermediate estimates $est.$, which are subsequently refined through DRS to obtain the HR latent representation z_{HR} . Finally, z_{HR} is passed to the VAE decoder to produce the high-quality HR output V_{HR} .

During training, we incorporate LoRA layers [15] into both the VAE encoder and diffusion UNet, achieving efficient parameter tuning while preserving generation priors. To ensure temporal consistency throughout the reconstruction process from V_{LR} to V_{HR} , we integrate the RTS module across multiple scales of both the diffusion UNet and VAE decoder, components identified as primary sources of temporal flickering artifacts in the original architecture [53, 62]. SJD is further used to enforce that the one-step reconstruction model generates the HR video V_{HR} with both spatial realism and temporal coherence. The detailed network structure of these models can be found in the supplementary materials. Furthermore, we also propose a Temporally Asynchronous Inference (TAI) strategy for memory-efficient long-range dependency modeling in Sec. 3.5.

3.2 Degradation-aware Reconstruction Scheduling

Standard diffusion models (DDPMs) [14, 34] assume a forward diffusion process that gradually adds noise to real data z_0 following a fixed noise schedule:

$$z_t = \sqrt{\bar{\alpha}_t} z_0 + \sqrt{1 - \bar{\alpha}_t} \epsilon, \quad (1)$$

where $t \in \{0, 1, 2, \dots, T\}$, $\bar{\alpha}_t = \prod_{i=0}^t \alpha_i$ is a hyperparameter controlling the noise strength. The reverse diffusion process iteratively denoises from z_T to z_0 , but this inherently results in computationally expensive inference.

Inspired by the consistency models [35] and one-step generation models [29, 40, 56] that map the point z_t on the diffusion trajectory to the starting point z_0 directly, we introduce DRS to enable a one-step reconstruction from LR latent z_{LR} to HR latent z_{HR} .

As shown in Fig. 3 (a), we first estimate a degradation factor $d \in [0, 1]$ to quantify the degradation severity of V_{LR} :

$$d = DEM(V_{LR}), \quad (2)$$

where the degradation estimation module (DEM) is implemented using the pretrained CLIP model [39], which is a widely used no-reference quality assessment model. Here, $d = 0$ corresponds to maximal video degradation, while $d = 1$ indicates minimal degradation. This is consistent with the diffusion process described in Eq. 1: a lower $\bar{\alpha}_t$ pushes z_t closer to Gaussian noise, whereas a higher $\bar{\alpha}_t$ retains stronger fidelity to the real data distribution. Therefore, we formulate a direct mapping between the degradation factor d and the noise schedule by defining $d = \sqrt{\bar{\alpha}_t}$, mathematically linking perceptual quality to the denoising process. In this way, the HR latent representation z_{HR} can be derived as:

$$z_{HR} = \frac{z_{LR} - \sqrt{1 - d^2} est.}{d}, \quad (3)$$

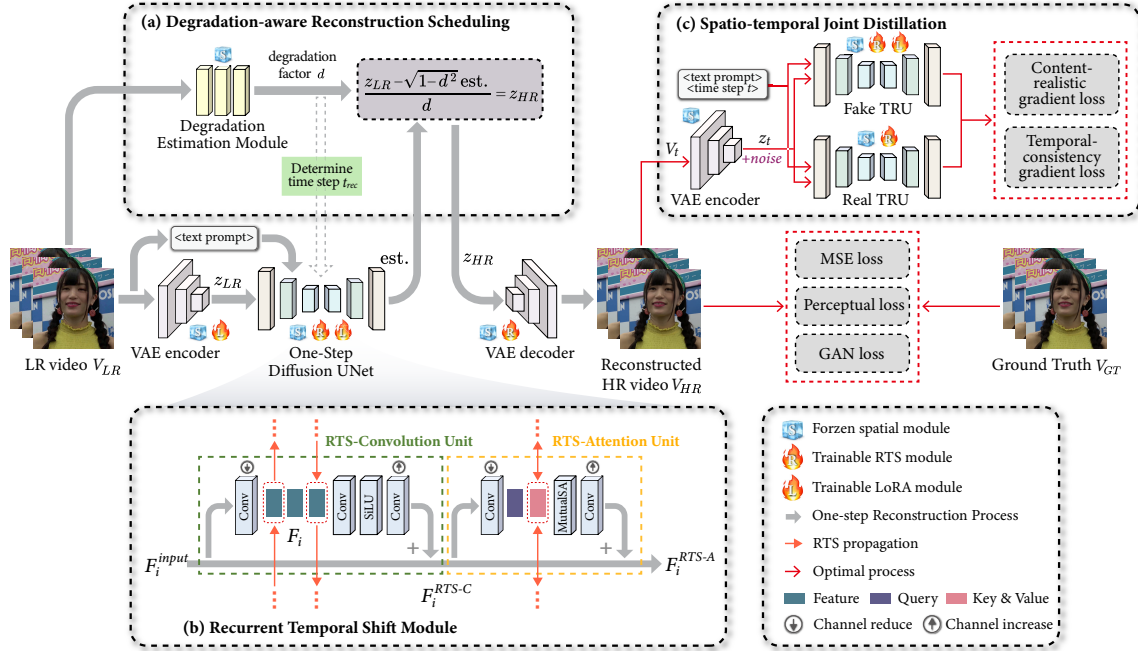


Figure 3: Training framework of the proposed UltraVSR.

where $est.$ denotes the diffusion UNet’s output.

Additionally, we determine the reconstruction time step t_{rec} through nearest-neighbor matching against the predefined noise schedule $\{\sqrt{\alpha_t}\}_{t=1}^T$:

$$t_{rec} = \arg \min_t |d - \sqrt{\alpha_t}|, \quad (4)$$

selecting the time step where $\sqrt{\alpha_{t_{rec}}}$ most closely approximates the degradation factor d . This mechanism enables efficient one-step reconstruction by leveraging the pretrained generative prior.

3.3 Recurrent Temporal Shift Module

The key to VSR lies in effectively aggregating complementary spatio-temporal information from misaligned frames. To this end, we propose a lightweight yet effective Recurrent Temporal Shift (RTS) module that captures spatio-temporal dependencies without relying on computationally expensive temporal layers. As illustrated in Fig.3 (b), the RTS module performs temporal feature propagation by bidirectionally shifting partitioned features across adjacent frames in a parameter-free manner, inspired by [4, 26, 27]. It consists of two core components: the RTS-Convolution Unit and the RTS-Attention Unit, which collaborate to enable efficient information exchange and fusion across neighboring frames. To further improve computational efficiency, we apply channel-reducing and channel-increasing convolutions at the beginning and end of each unit, respectively.

3.3.1 RTS-Convolution Unit. Given an intermediate feature map $F_i = \text{Conv}(F_i^{input}) \in \mathbb{R}^{C \times h \times w}$ for the i -th frame, RTS divides it into three equal channel-wise segments: F_i^{-1} , F_i^0 , and F_i^1 , where each segment $F_i^j \in \mathbb{R}^{T \times \frac{C}{3} \times h \times w}$. These segments are then shifted along the temporal dimension with offsets of +1, 0, and -1, respectively, where a positive offset denotes a forward shift, a negative offset

denotes a backward shift, and zero implies no shift. The aggregated features for the i -th frame are then obtained by concatenating the temporally shifted feature segments:

$$F_i^{Agg} = \text{Concat}(F_{i-1}^{-1}, F_i^0, F_{i+1}^1). \quad (5)$$

This strategy ensures that each frame receives contextual information from both past and future frames. To maintain consistent dimensions throughout the video, zero-padding is applied at the sequence boundaries. The aggregated features are processed via convolutional layers with ReLU activation followed by a residual connection to perform local temporal alignment:

$$F_i^{RTS-C} = \text{Conv}(\text{ReLU}(\text{Conv}(F_i^{Agg}))) + F_i^{input}. \quad (6)$$

3.3.2 RTS-Attention Unit. Building on the observation that attention-based feature alignment inherently captures strong semantic priors in diffusion models [2, 4, 11, 36], we further develop an RTS-attention unit to aggregate high-level global contextual dependencies across frames. Given the *Query*, *Key*, and *Value* embeddings $\{Q_i, K_i, V_i\} = \text{Conv}(F_i^{RTS-C})$ for the i -th frame, RTS shifts K_i and V_i forward and backward temporally, allowing the model to query semantically correlated structures and textures from adjacent frames. We adopt Mutual Self-Attention (MutualSA) [4] to aggregate semantic information across frames:

$$F_i^{MSA} = \sum_{j=-1}^1 \text{MutualSA}(Q_i, K_{i+j}, V_{i+j}), \quad (7)$$

where $\text{MutualSA}(Q_i, K_{i+j}, V_{i+j}) = \text{Softmax}(\frac{Q_i K_{i+j}^T}{\sqrt{r}}) V_{i+j}$, r denotes the embedding dimension. The final output of the RTS-Attention Unit is obtained by:

$$F_i^{RTS-A} = \text{Conv}(F_i^{MSA}) + F_i^{RTS-C}. \quad (8)$$

Unlike conventional spatial self-attention, which operates independently on each frame, the RTS-attention unit aligns semantic information across the temporal dimension, thereby enhancing the temporal consistency of the reconstructed video.

3.4 Spatio-temporal Joint Distillation

To guide the proposed one-step reconstruction in generating visually realistic and temporally consistent HR videos, we introduce a dual-constrained optimization strategy, termed Spatio-temporal Joint Distillation (SJD). Our SJD shares motivation with other distribution matching generative models, such as SDS [31] and VSD [44, 56], but extends these paradigms from the image domain to video, explicitly modeling inter-frame temporal consistency dependencies.

As illustrated in Fig.3 (c), SJD introduces two Temporal Regularized UNets (TRU), a real TRU $\mathcal{T}_{\text{real}}$ and a fake TRU $\mathcal{T}_{\text{fake}}$. They are derived by integrating our proposed RTS module into the Stable Diffusion model [32]. During the training of the one-step reconstruction model G_θ , $\mathcal{T}_{\text{real}}$ and $\mathcal{T}_{\text{fake}}$ are dynamically updated using ground-truth video V_{GT} and the synthesized output V_{HR} , respectively. To capture both spatial realism and temporal consistency, we convert the noise predictions into video distributions using Eq. 1 at the output of the TRUs. Conceptually, $\mathcal{T}_{\text{real}}$ can be interpreted as providing gradient directions that encourage the reconstruction to become more realistic and temporally coherent. In contrast, $\mathcal{T}_{\text{fake}}$ yields gradients that reflect undesirable characteristics such as visual artifacts and temporal flickering. To this end, we formulate the gradient update rule for G_θ by integrating a content-realistic gradient loss and a temporal-consistency gradient loss:

$$\nabla \mathcal{L}_{\text{SJD}} = \nabla \mathcal{L}_{\text{realistic}} + \lambda \nabla \mathcal{L}_{\text{consistency}}, \quad (9)$$

where λ balances content realism and temporal coherence of V_{HR} . This encourages the synthesized V_{HR} toward higher perceptual realism and temporal coherence while suppressing visual artifacts and flickering. Specifically, the content-realistic gradient loss is formulated as:

$$\nabla \mathcal{L}_{\text{realistic}} = \mathbb{E} \left[\omega(t) (\mathcal{T}_{\text{real}}(z_t, t) - \mathcal{T}_{\text{fake}}(z_t, t)) \frac{dG}{d\theta} \right], \quad (10)$$

where $z_t = \sqrt{\alpha_t} z_0 + \sqrt{1 - \alpha_t} \epsilon$, $z_0 = \mathcal{E}(V_{HR})$, $V_{HR} = G_\theta(V_{LR})$, $\epsilon \sim \mathcal{N}(0, \mathbf{I})$, \mathcal{E} denotes the pretrained VAE encoder, $\omega(t)$ is a weighting coefficient to normalize the gradient magnitudes across varying noise levels [56]. The temporal-consistency gradient loss enhances temporal coherence by penalizing discrepancies in the inter-frame gradients of two TRUs:

$$\nabla \mathcal{L}_{\text{consistency}} = \mathbb{E} \left[\omega(t) \left((\mathcal{T}_{\text{real}}(z_t, t)[:-1] - \mathcal{T}_{\text{real}}(z_t, t)[1:]) \right. \right. \\ \left. \left. - (\mathcal{T}_{\text{fake}}(z_t, t)[:-1] - \mathcal{T}_{\text{fake}}(z_t, t)[1:]) \right) \frac{dG}{d\theta} \right]. \quad (11)$$

3.5 Temporally Asynchronous Inference

Existing diffusion-based VSR methods exhibit critical dependencies on temporal modules, incurring prohibitive memory overheads. As a result, such models require video segmentation into short clips for piecewise processing, as shown in Fig. 4 (a). For instance,

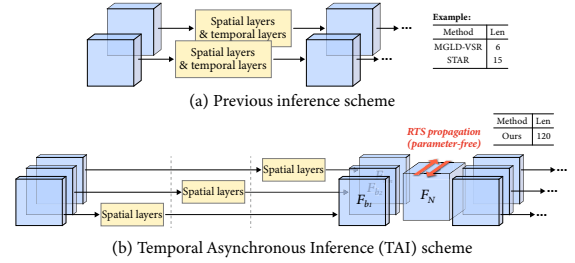


Figure 4: The previous inference scheme vs. the proposed Temporally Asynchronous Inference (TAI) scheme.

under 48GB GPU memory constraints (NVIDIA RTX 8000), MGLD-VSR [53] processes ≤ 6 frames while STAR [49] handles ≤ 15 frames for 2K (1440×2560) reconstruction. This fragmentation disrupts temporal continuity and fundamentally limits long-range dependency modeling. UltraVSR circumvents this limitation through implicit temporal modeling via RTS propagation, eliminating explicit temporal layers. Building on this architectural innovation, we propose a Temporally Asynchronous Inference (TAI) strategy that enables efficient capture of long-range temporal dependencies.

As illustrated in Fig. 4 (b), given an N -frames low-resolution video V_{LR} , TAI first divides it into m non-overlapping sub-sequences $\{V_{LR_1}, V_{LR_2}, \dots, V_{LR_m}\}$, each containing b frames. Then, these sub-sequences are processed sequentially through 2D spatial layers to obtain feature maps $\{F_{b_1}, F_{b_2}, \dots, F_{b_m}\}$, drastically reducing peak memory consumption. At the beginning of the RTS propagation, all these features are concatenated into a unified feature tensor F_N , which is then augmented by bidirectional RTS propagation to achieve efficient temporal information exchange between frames. The temporally shifted features are then divided back into sub-sequences for further refinement.

As a result, TAI enables memory-efficient inference while maintaining long-term temporal dependencies, capable of processing up to 120 frames at 1440×2560 resolution identical hardware constraints, an 8× throughput improvement over STAR [49]. This breakthrough makes UltraVSR particularly suitable for high-quality reconstruction of long-duration video sequences under resource-limited environments.

4 EXPERIMENTS

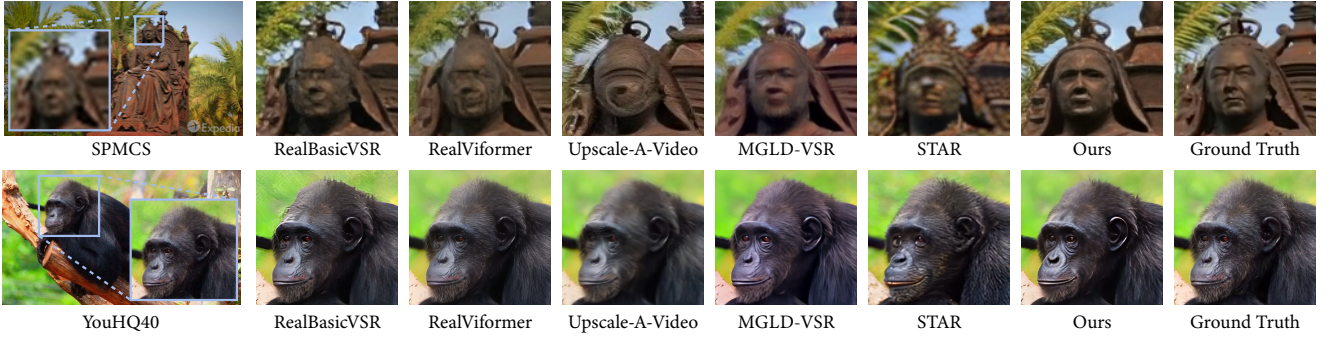
4.1 Experimental Settings

4.1.1 Datasets. Similar to the most VSR approaches [7, 53, 60], we combine the training and validation sets from the REDS dataset [28] for model training, reserving four sequences (REDS4) for testing. We evaluate UltraVSR on four synthetic datasets (i.e., REDS4, SPMCS [55], UDM10 [37], and YouHQ40 [62]) and a real-world dataset (i.e., VideoLQ [7]) that contains 50 real-world video sequences with diverse degradations. For both synthetic training and testing datasets, LR-HR video pairs are generated following the degradation pipeline of RealBasicVSR [7].

4.1.2 Training Details. We implement UltraVSR using the PyTorch framework and the Diffusers [30] library. The input sequence length is set to 6, with the spatial size cropped to 512×512 resolution. We freeze the original spatial modules of the pretrained Stable Diffusion model to preserve its generation priors, while only training the

Table 1: Quantitative comparison with state-of-the-art VSR approaches on both synthetic and real-world benchmarks. The best and second best results are **highlighted and underlined, respectively.**

| Datasets | Metrics | BasicVSR++ [6] | OVSR [54] | RealBasicVSR [7] | VRT [24] | RealViformer [60] | Upscale-A-Video [62] | MGLD-VSR [33] | STAR [49] | Ours |
|----------|----------|----------------|---------------|------------------|---------------|-------------------|----------------------|---------------|---------------|---------------|
| REDS4 | PSNR | 33.77 | 23.55 | 28.59 | 32.97 | 28.18 | 25.62 | 27.49 | 24.08 | 24.50 |
| | SSIM | 0.9173 | 0.6743 | 0.8066 | <u>0.9007</u> | 0.7896 | 0.6761 | 0.7783 | 0.6721 | 0.6962 |
| | MUSIQ | 67.00 | 54.44 | 67.03 | 65.68 | 64.58 | 32.30 | 58.94 | 60.94 | 70.07 |
| | CLIP-IQA | 0.3149 | 0.3383 | 0.3724 | <u>0.3743</u> | 0.3558 | 0.1843 | 0.2908 | 0.3047 | 0.4397 |
| | MANIQA | <u>0.6752</u> | 0.5887 | 0.6671 | 0.6699 | 0.6545 | 0.3138 | 0.5837 | 0.6123 | 0.6821 |
| | DOVER | 0.7182 | 0.6620 | 0.7209 | 0.7067 | 0.7152 | 0.4053 | 0.6717 | <u>0.7227</u> | 0.7304 |
| SPMCS | PSNR | 23.39 | 29.87 | 22.87 | 23.43 | 23.45 | <u>24.10</u> | 23.43 | 22.95 | 23.08 |
| | SSIM | 0.6516 | 0.8702 | 0.6087 | <u>0.6543</u> | 0.6153 | 0.6386 | 0.6372 | 0.6001 | 0.6202 |
| | MUSIQ | 62.57 | 57.10 | <u>69.44</u> | 63.44 | 66.10 | 56.31 | 64.08 | 55.14 | 69.92 |
| | CLIP-IQA | 0.4341 | 0.4597 | <u>0.4838</u> | 0.4388 | 0.4432 | 0.3353 | 0.4685 | 0.3888 | 0.5377 |
| | MANIQA | 0.6263 | 0.6057 | <u>0.6282</u> | 0.6134 | 0.6148 | 0.4798 | 0.5562 | 0.5640 | 0.6386 |
| | DOVER | 0.6711 | 0.6031 | <u>0.7506</u> | 0.6404 | 0.7206 | 0.5675 | 0.6431 | 0.6404 | 0.7616 |
| UDM10 | PSNR | 34.68 | 27.12 | 31.31 | 36.03 | 31.84 | 29.48 | 29.50 | 27.93 | 27.96 |
| | SSIM | <u>0.9406</u> | 0.8318 | 0.8936 | 0.9501 | 0.9074 | 0.8458 | 0.8744 | 0.8284 | 0.8346 |
| | MUSIQ | 63.26 | 57.94 | <u>66.01</u> | 61.38 | 61.86 | 39.48 | 64.54 | 57.34 | 66.46 |
| | CLIP-IQA | 0.5091 | 0.4338 | 0.4903 | 0.4697 | 0.4356 | 0.2356 | <u>0.5083</u> | 0.3843 | 0.4818 |
| | MANIQA | 0.5729 | 0.5593 | <u>0.6083</u> | 0.5501 | 0.5699 | 0.3329 | 0.5495 | 0.5219 | 0.6167 |
| | DOVER | 0.7947 | 0.7789 | <u>0.8248</u> | 0.7709 | 0.8185 | 0.5500 | 0.7851 | 0.8061 | 0.8361 |
| YouHQ40 | PSNR | 23.99 | 22.67 | <u>25.26</u> | 25.01 | 25.73 | 25.20 | 24.97 | 23.76 | 24.75 |
| | SSIM | 0.5999 | 0.5670 | 0.6857 | 0.6510 | <u>0.6974</u> | 0.6865 | 0.6984 | 0.6593 | 0.6954 |
| | MUSIQ | 49.43 | 45.54 | 62.12 | 41.45 | <u>62.27</u> | 35.86 | 56.42 | 41.47 | 62.71 |
| | CLIP-IQA | 0.3798 | 0.3442 | <u>0.4661</u> | 0.3879 | 0.4520 | 0.2460 | 0.3960 | 0.3435 | 0.4928 |
| | MANIQA | 0.5145 | 0.4710 | <u>0.5539</u> | 0.4622 | 0.5500 | 0.3401 | 0.4717 | 0.4198 | 0.5847 |
| | DOVER | 0.6914 | 0.6877 | <u>0.8855</u> | 0.6347 | 0.8657 | 0.6216 | 0.8116 | 0.8084 | 0.8872 |
| VideoLQ | MUSIQ | 37.32 | 29.89 | <u>62.48</u> | 37.94 | 58.66 | 30.88 | 55.99 | 54.59 | 64.42 |
| | CLIP-IQA | 0.2766 | 0.2875 | <u>0.3663</u> | 0.2763 | 0.3211 | 0.1817 | 0.3385 | 0.3126 | 0.4599 |
| | MANIQA | 0.4099 | 0.3447 | <u>0.5721</u> | 0.4051 | 0.5477 | 0.3025 | 0.5004 | 0.5507 | 0.5907 |
| | DOVER | 0.5128 | 0.5141 | <u>0.7645</u> | 0.5136 | 0.7399 | 0.4493 | 0.7254 | 0.7034 | 0.7785 |

**Figure 5: Visual comparisons on synthetic low-quality videos from SPMCS [55] and YouHQ40 [62] datasets.**

newly introduced LoRA and RTS modules. Adam [20] optimizer is employed as the optimizer with $\beta_1 = 0.9$ and $\beta_2 = 0.99$. We use a combination of MSE loss, perceptual loss, temporal GAN loss [61], and SJD regularization loss to train UltraVSR. The real and fake TRUs are trained by minimizing a standard denoising objective [14, 38]. The weighting coefficient λ is set to 0.5. The initial learning rate is set to 5×10^{-5} for all models.

4.1.3 Evaluation Metrics. We evaluate super-resolved video quality using three image-based quality metrics: MUSIQ [19], CLIP-IQA [39], and MANIQA [52], along with one video-specific quality metric, DOVER [45]. DOVER assesses both content quality and temporal consistency from both aesthetic and technical perspectives. In addition, the full-reference metrics (i.e., PSNR and SSIM) are also given as a reference. However, it should be noted that they only reflect certain aspects of performance and poorly respond to realistic visuals [3, 12, 17, 21, 57], which can not reliably evaluate the performance of diffusion-based VSR models.

4.2 Evaluation with State-of-the-art Methods

To validate the efficacy of UltraVSR, we conduct both quantitative and qualitative comparisons with several state-of-the-art VSR methods: BasicVSR++ [6], OVSR [54], RealBasicVSR [7], VRT [24], RealViformer [60], Upscale-A-Video [62], MGLD-VSR [33], and STAR [49]. For a more comprehensive evaluation, we also include comparisons with state-of-the-art SISR approaches (i.e., RealESRGAN [42], StableSR [41], SUPIR [57], ResShift [58] and OSediff [46]) in the supplementary materials.

4.2.1 Quantitative Comparison. As demonstrated in Tab. 1, we present the quantitative results with existing state-of-the-art VSR approaches. It can be seen that our UltraVSR consistently achieves the highest score across nearly all non-reference metrics on all synthetic benchmarks, demonstrating its superior performance. Although approaches like BasicVSR++ [6] and VRT [24] have better performance in terms of PSNR or SSIM, they usually produce unsatisfactory results on real-world degraded videos (see Sec. 4.2.2),

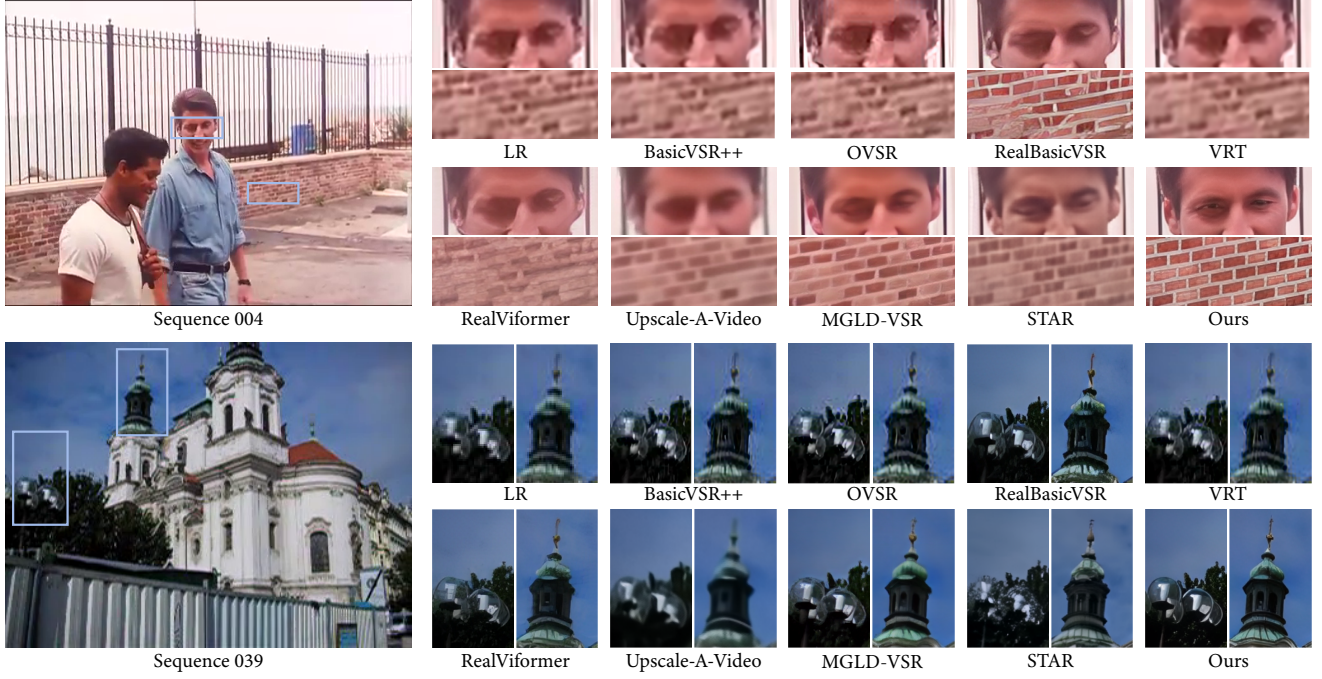


Figure 6: Visual comparisons on real-world low-quality videos from VideoLQ [7] dataset.

Table 2: Efficiency evaluations among diffusion-based VSR approaches. Note that the runtime is evaluated using a single RTX 8000 GPU. Both trainable/total parameters are measured for each model. The best results are highlighted.

| Methods | Sampling step | Runtime (s) | | # Params (M) |
|----------------------|---------------|-------------|-------------|------------------|
| | | 720×1280 | 1440×2560 | |
| Upscale-A-Video [62] | 30 | 16.1 | 32.0 | ~ 96.6/746 |
| MGLD-VSR [33] | 50 | 31.8 | 204 | 156.0/1465 |
| STAR [49] | 15 | 14.5 | 110.2 | 629.9/2139 |
| Ours | 1 | 0.89 | 2.67 | 10.5/1912 |

as reflected in their lower no-reference metric scores. As for real-world VSR dataset VideoLQ [7], UltraVSR outperforms other methods across all non-reference metrics (MUSIQ: **+1.94**, CLIP-IQA: **+0.0936**, MANIQA: **+0.0186**, DOVER: **+0.014**). These notable improvements highlight UltraVSR’s strong ability to enhance complex and diverse real-world videos while preserving realistic details.

4.2.2 Qualitative Comparison. To further assess the effectiveness of the proposed UltraVSR, we present qualitative comparisons on both synthetic datasets (SPMCS [55] and YouHQ40 [62] in Fig. 5) and real-world dataset (VideoLQ [7] in Fig. 6). On synthetic videos, it can be observed that the competing approaches struggle to reconstruct accurate texture (e.g., the results of Upscale-A-Video [62] and STAR [49] in the first row) and blurriness (e.g., the results of RealViFormer [60] and the result of Upscale-A-Video [62] in the second row). In addition, MGLD-VSR [33] introduces color artifacts in the reconstructed frames. In contrast, our UltraVSR excels in restoring lost textures and structures under complex degradation scenarios, such as the outlines of statues and animal fur. On real-world videos, UltraVSR generates high-quality texture information that surpasses those of competing approaches. For instance, in sequence 004, UltraVSR not only recovers clear and realistic facial expressions but

also reconstructs plausible exterior structure of the surrounding brick wall. In sequence 039, UltraVSR successfully restores intricate architectural details and decorations, demonstrating its strong robustness and generalization ability under challenging degradation scenarios. More comparisons can be found in the supplementary materials.

4.2.3 Temporal Consistency. A key challenge in VSR is maintaining temporal consistency across frames. From a quantitative perspective, we compare the DOVER metric, an effective video quality assessment approach, against competing methods in Tab. 1. Due to the inherent randomness in the diffusion model, the DOVER scores of existing diffusion-based VSR methods are generally low. Benefiting from the proposed one-step diffusion space, our UltraVSR achieves the best score on all the datasets (e.g., **+0.011** on the SPMCS dataset and **+0.014** on the VideoLQ dataset). In addition, Fig. 7 presents visual comparisons against both SISr and VSR approaches. It can be found that due to the inherent randomness and insufficient temporal modeling, results from SUPIR [57] and OSEDiff [46] exhibit severe temporal inconsistencies. While existing VSR approaches alleviate this issue, they often sacrifice texture details. In contrast, our ultraVSR successfully reconstructs videos with both fine texture structure and temporal coherence.

4.2.4 Efficiency Evaluations. To evaluate the efficiency of UltraVSR, we compare its sampling step, runtime, and parameters against other diffusion-based VSR approaches in Tab. 2. we assess computational efficiency at two common resolutions: 720p (720×1280) and 2K (1440×2560). All models were evaluated on a single NVIDIA RTX 8000 GPU. Existing diffusion-based VSR approaches typically require dozens of iterative sampling steps, resulting in prohibitively

Table 3: Ablation study of different configurations. Both trainable/total parameters of the one-step reconstruction model are measured for each model variant. The best and second best results are **highlighted and underlined, respectively.**

| Models | DRS | RTS-Convolution Unit | RTS-Attention Unit | VSD [44, 56] | SJD | TAI | MUSIQ | CLIP-IQA | MANIQA | DOVER | # Params (M) |
|--------|-----|----------------------|--------------------|--------------|-----|-----|---------------|---------------|--------------|---------------|--------------|
| A | | | | ✓ | | ✓ | 0.5707 | 0.4360 | 61.93 | 0.7571 | 4.4/1804 |
| B | ✓ | | | ✓ | | ✓ | 0.5759 | 0.4467 | 63.86 | 0.7564 | 4.4/1906 |
| C | ✓ | ✓ | | ✓ | | ✓ | 0.5792 | 0.4547 | 63.93 | 0.7676 | 7.3/1909 |
| D | ✓ | ✓ | ✓ | ✓ | | ✓ | 0.5824 | <u>0.4572</u> | <u>64.25</u> | <u>0.7704</u> | 10.5/1912 |
| E | ✓ | ✓ | ✓ | | ✓ | ✓ | <u>0.5851</u> | <u>0.4524</u> | <u>64.09</u> | <u>0.7665</u> | 10.5/1912 |
| Ours | ✓ | ✓ | ✓ | | ✓ | ✓ | 0.5907 | 0.4599 | 64.42 | 0.7785 | 10.5/1912 |

**Figure 7: Temporal consistency analysis across various approaches, including both **SISR** and **VSR** approaches, as well as different **model variants**.**

long inference times, especially for 2K video, making them impractical for real-world deployment. Thanks to the efficient one-step diffusion space, our UltraVSR significantly reduces inference time, taking only **0.06×** and **0.08×** that of the second fastest approach at two resolutions. Moreover, UltraVSR has substantially fewer trainable parameters (just **10.5M**) compared to other diffusion-based methods, underscoring its efficiency during the training process.

4.3 Ablation Study

We conduct comprehensive quantitative and qualitative experiments to evaluate the contributions of the key components in UltraVSR. The ablation results are presented in Tab. 3, with exemplar visual comparisons shown in Fig. 7. We begin with Model A, which serves as our baseline, constructed by: (1) fixing the diffusion time step to 999, following the one-step generation paradigm established in prior works [9, 29, 50, 56]; (2) enabling only the trainable LoRA layers; and (3) replacing our proposed Spatio-temporal Joint Distillation (SJD) with the conventional Variational Score Distillation (VSD) [44, 56]. Due to its inability to dynamically perceive degradation levels, Model A exhibits limited reconstruction quality compared to Model B (with DRS). Next, we progressively

enhance Model B by introducing trainable RTS-convolution and RTS-attention units, resulting in Model C and Model D, respectively. Thanks to the strong temporal modeling capability of RTS, inter-frame consistency improves steadily across these models. We further evaluate the effectiveness of SJD and Temporally Asynchronous Inference (TAI) by comparing Model D, Model E (where a fixed local sequence of length 10 is used), and our model. It can be seen that SJD significantly enhances temporal coherence by introducing inter-frame difference supervision, leading to improved motion continuity across frames compared to VSD [44, 56]. Moreover, TAI further boosts performance by enabling long-range temporal modeling. These results collectively demonstrate the necessity and effectiveness of each proposed component in UltraVSR.

5 DISCUSSION

While UltraVSR introduces an efficient one-step VSR framework that greatly reduces the computational cost, it is still challenging to deploy it on multimedia applications with high real-time requirements. We will explore hardware-aware acceleration on different deployment platforms in future work.

6 CONCLUSION

We present UltraVSR, the first work to address real-world VSR through an efficient one-step diffusion framework. To enable this, we propose Degradation-aware Reconstruction Scheduling (DRS), which transforms the conventional multi-step denoising into a one-step LR-to-HR reconstruction. To maintain temporal consistency, we develop the Recurrent Temporal Shift (RTS) module for efficient feature propagation, fusion, and alignment. We further introduce Spatio-temporal Joint Distillation (SJD) for realistic and coherent outputs, and Temporally Asynchronous Inference (TAI) for efficient long-range temporal modeling. Extensive experiments show that UltraVSR delivers favorable performance with significantly accelerated inference speed.

REFERENCES

- [1] Zekun Ai, Xiaotong Luo, Yanyun Qu, and Yuan Xie. 2024. SkipVSR: Adaptive Patch Routing for Video Super-Resolution with Inter-Frame Mask. In *Proceedings of the 32nd ACM International Conference on Multimedia*. 5874–5882.
- [2] Yuval Alaluf, Daniel Garibi, Or Patashnik, Hadar Averbuch-Elor, and Daniel Cohen-Or. 2024. Cross-image attention for zero-shot appearance transfer. In *ACM SIGGRAPH 2024 Conference Papers*. 1–12.
- [3] Yochai Blau and Tomer Michaeli. 2018. The perception-distortion tradeoff. In *Proceedings of the IEEE conference on computer vision and pattern recognition*. 6228–6237.
- [4] Mingdeng Cao, Xintao Wang, Zhongang Qi, Ying Shan, Xiaohe Qie, and Yinqiang Zheng. 2023. Masactrl: Tuning-free mutual self-attention control for consistent image synthesis and editing. In *Proceedings of the IEEE/CVF international conference on computer vision*. 22560–22570.
- [5] Kelvin CK Chan, Xintao Wang, Ke Yu, Chao Dong, and Chen Change Loy. 2021. Basicvsr: The search for essential components in video super-resolution and beyond. In *Proceedings of the IEEE/CVF conference on computer vision and pattern recognition*. 4947–4956.
- [6] Kelvin CK Chan, Shangchen Zhou, Xiangyu Xu, and Chen Change Loy. 2022. Basicvsr++: Improving video super-resolution with enhanced propagation and alignment. In *Proceedings of the IEEE/CVF conference on computer vision and pattern recognition*. 5972–5981.
- [7] Kelvin CK Chan, Shangchen Zhou, Xiangyu Xu, and Chen Change Loy. 2022. Investigating tradeoffs in real-world video super-resolution. In *Proceedings of the IEEE/CVF Conference on Computer Vision and Pattern Recognition*. 5962–5971.
- [8] Prafulla Dhariwal and Alexander Nichol. 2021. Diffusion models beat gans on image synthesis. *Advances in neural information processing systems* 34 (2021), 8780–8794.
- [9] Kevin Frans, Danijar Hafner, Sergey Levine, and Pieter Abbeel. 2024. One step diffusion via shortcut models. *arXiv preprint arXiv:2410.12557* (2024).
- [10] Dario Fuoli, Shuhang Gu, and Radu Timofte. 2019. Efficient video super-resolution through recurrent latent space propagation. In *2019 IEEE/CVF International Conference on Computer Vision Workshop (ICCVW)*. IEEE, 3476–3485.
- [11] Michal Geyer, Omer Bar-Tal, Shai Bagon, and Tali Dekel. 2023. Tokenflow: Consistent diffusion features for consistent video editing. *arXiv preprint arXiv:2307.10373* (2023).
- [12] Jinjin Gu, Haoming Cai, Chao Dong, Jimmy S Ren, Radu Timofte, Yuan Gong, Shanshan Lao, Shuwei Shi, Jiahao Wang, Sidi Yang, et al. 2022. NTIRE 2022 challenge on perceptual image quality assessment. In *Proceedings of the IEEE/CVF conference on computer vision and pattern recognition*. 951–967.
- [13] Akash Gupta, Padmaja Jonnalagedda, Bir Bhanu, and Amit K Roy-Chowdhury. 2021. Ada-vsr: Adaptive video super-resolution with meta-learning. In *Proceedings of the 29th ACM international conference on multimedia*. 327–336.
- [14] Jonathan Ho, Ajay Jain, and Pieter Abbeel. 2020. Denoising diffusion probabilistic models. *Advances in neural information processing systems* 33 (2020), 6840–6851.
- [15] Edward J Hu, Yelong Shen, Phillip Wallis, Zeyuan Allen-Zhu, Yanzhi Li, Shean Wang, Lu Wang, Weizhu Chen, et al. 2022. Lora: Low-rank adaptation of large language models. *ICLR* 1, 2 (2022), 3.
- [16] Shuo Jin, Meiqin Liu, Chao Yao, Chunyu Lin, and Yao Zhao. 2023. Kernel dimension matters: To activate available kernels for real-time video super-resolution. In *Proceedings of the 31st ACM International Conference on Multimedia*. 8617–8625.
- [17] Gu Jinjin, Cai Haoming, Chen Haoyu, Ye Xiaoxing, Jimmy S Ren, and Dong Chao. 2020. Pipal: a large-scale image quality assessment dataset for perceptual image restoration. In *Computer Vision—ECCV 2020: 16th European Conference, Glasgow, UK, August 23–28, 2020, Proceedings, Part XI* 16. Springer, 633–651.
- [18] Bahjat Kawar, Shiran Zada, Oran Lang, Omer Tov, Huiwen Chang, Tali Dekel, Inbar Mosseri, and Michal Irani. 2023. Imagic: Text-based real image editing with diffusion models. In *Proceedings of the IEEE/CVF conference on computer vision and pattern recognition*. 6007–6017.
- [19] Junjie Ke, Qifei Wang, Yilin Wang, Peyman Milanfar, and Feng Yang. 2021. Musiq: Multi-scale image quality transformer. In *Proceedings of the IEEE/CVF international conference on computer vision*. 5148–5157.
- [20] Diederik P Kingma and Jimmy Ba. 2014. Adam: A method for stochastic optimization. *arXiv preprint arXiv:1412.6980* (2014).
- [21] Christian Ledig, Lucas Theis, Ferenc Huszar, Jose Caballero, Andrew Cunningham, Alejandro Acosta, Andrew Aitken, Alykhan Tejani, Johannes Totz, Zehan Wang, et al. 2017. Photo-realistic single image super-resolution using a generative adversarial network. In *Proceedings of the IEEE conference on computer vision and pattern recognition*. 4681–4690.
- [22] Jiaxu Leng, Jia Wang, Xinbo Gao, Bo Hu, Ji Gan, and Chenqiang Gao. 2022. Icnr: Joint alignment and reconstruction via iterative collaboration for video super-resolution. In *Proceedings of the 30th ACM International Conference on Multimedia*. 6675–6684.
- [23] Dasong Li, Xiaoyu Shi, Yi Zhang, Ka Chun Cheung, Simon See, Xiaogang Wang, Hongwei Qin, and Hongsheng Li. 2023. A simple baseline for video restoration with grouped spatial-temporal shift. In *Proceedings of the IEEE/CVF Conference on Computer Vision and Pattern Recognition*. 9822–9832.
- [24] Jingyun Liang, Jiezhang Cao, Yuchen Fan, Kai Zhang, Rakesh Ranjan, Yawei Li, Radu Timofte, and Luc Van Gool. 2024. Vrt: A video restoration transformer. *IEEE Transactions on Image Processing* (2024).
- [25] Jingyun Liang, Yuchen Fan, Xiaoyu Xiang, Rakesh Ranjan, Eddy Ilg, Simon Green, Jiezhang Cao, Kai Zhang, Radu Timofte, and Luc V Gool. 2022. Recurrent video restoration transformer with guided deformable attention. *Advances in Neural Information Processing Systems* 35 (2022), 378–393.
- [26] Ji Lin, Chuang Gan, and Song Han. 2019. Tsm: Temporal shift module for efficient video understanding. In *Proceedings of the IEEE/CVF international conference on computer vision*. 7083–7093.
- [27] Andres Munoz, Mohammadreza Zolfaghari, Max Argus, and Thomas Brox. 2021. Temporal shift GAN for large scale video generation. In *Proceedings of the IEEE/CVF Winter Conference on Applications of Computer Vision*. 3179–3188.
- [28] Seungjun Nah, Sungyong Baik, Seokil Hong, Gyeongsik Moon, Sanghyun Son, Radu Timofte, and Kyoung Mu Lee. 2019. Ntire 2019 challenge on video deblurring and super-resolution: Dataset and study. In *Proceedings of the IEEE/CVF conference on computer vision and pattern recognition workshops*. 0–0.
- [29] Thuan Hoang Nguyen and Anh Tran. 2024. Swiftbrush: One-step text-to-image diffusion model with variational score distillation. In *Proceedings of the IEEE/CVF Conference on Computer Vision and Pattern Recognition*. 7807–7816.
- [30] Anton Lozhkov Pedro Cuenca Nathan Lambert Kashif Rasul Mishig Davaadorj Patrick von Platen, Suraj Patil and Thomas Wolf. 2022. Diffusers: State-of-the-art Diffusion Models.
- [31] Ben Poole, Ajay Jain, Jonathan T Barron, and Ben Mildenhall. 2022. Dreamfusion: Text-to-3d using 2d diffusion. *arXiv preprint arXiv:2209.14988* (2022).
- [32] Robin Rombach, Andreas Blattmann, Dominik Lorenz, Patrick Esser, and Björn Ommer. 2022. High-resolution image synthesis with latent diffusion models. In *Proceedings of the IEEE/CVF conference on computer vision and pattern recognition*. 10684–10695.
- [33] Xiaoyu Shi, Zhaoyang Huang, Fu-Yun Wang, Weikang Bian, Dasong Li, Yi Zhang, Manyuan Zhang, Ka Chun Cheung, Simon See, Hongwei Qin, et al. 2024. Motion-i2v: Consistent and controllable image-to-video generation with explicit motion modeling. In *ACM SIGGRAPH 2024 Conference Papers*. 1–11.
- [34] Jascha Sohl-Dickstein, Eric Weiss, Niru Maheswaranathan, and Surya Ganguli. 2015. Deep unsupervised learning using nonequilibrium thermodynamics. In *International conference on machine learning*. PMLR, 2256–2265.
- [35] Yang Song, Prafulla Dhariwal, Mark Chen, and Ilya Sutskever. 2023. Consistency models. (2023).
- [36] Luming Tang, Menglin Jia, Qianqian Wang, Cheng Perng Phoo, and Bharath Hariharan. 2023. Emergent correspondence from image diffusion. *Advances in Neural Information Processing Systems* 36 (2023), 1363–1389.
- [37] Xin Tao, Hongyun Gao, Renjie Liao, Jue Wang, and Jiaya Jia. 2017. Detail-revealing deep video super-resolution. In *Proceedings of the IEEE international conference on computer vision*. 4472–4480.
- [38] Pascal Vincent. 2011. A connection between score matching and denoising autoencoders. *Neural computation* 23, 7 (2011), 1661–1674.
- [39] Jianyi Wang, Kelvin CK Chan, and Chen Change Loy. 2023. Exploring clip for assessing the look and feel of images. In *Proceedings of the AAAI conference on artificial intelligence*, Vol. 37. 2555–2563.
- [40] Jiangang Wang, Qingnan Fan, Qi Zhang, Haigen Liu, Yuhang Yu, Jinwei Chen, and Wenqi Ren. 2024. Hero-SR: One-Step Diffusion for Super-Resolution with Human Perception Priors. *arXiv preprint arXiv:2412.07152* (2024).
- [41] Jianyi Wang, Zongsheng Yue, Shangchen Zhou, Kelvin CK Chan, and Chen Change Loy. 2024. Exploiting diffusion prior for real-world image super-resolution. *International Journal of Computer Vision* (2024), 1–21.
- [42] Xintao Wang, Liangbin Xie, Chao Dong, and Ying Shan. 2021. Real-esrgan: Training real-world blind super-resolution with pure synthetic data. In *Proceedings of the IEEE/CVF international conference on computer vision*. 1905–1914.

- [43] Yufei Wang, Wenhan Yang, Xinyuan Chen, Yaohui Wang, Lanqing Guo, Lap-Pui Chau, Ziwei Liu, Yu Qiao, Alex C Kot, and Bihan Wen. 2024. Sinsr: diffusion-based image super-resolution in a single step. In *Proceedings of the IEEE/CVF conference on computer vision and pattern recognition*. 25796–25805.
- [44] Zhengyi Wang, Cheng Lu, Yikai Wang, Fan Bao, Chongxuan Li, Hang Su, and Jun Zhu. 2023. Prolificdreamer: High-fidelity and diverse text-to-3d generation with variational score distillation. *Advances in Neural Information Processing Systems* 36 (2023), 8406–8441.
- [45] Haoning Wu, Erli Zhang, Liang Liao, Chaofeng Chen, Jingwen Hou, Annan Wang, Wenxiu Sun, Qiong Yan, and Weisi Lin. 2023. Exploring video quality assessment on user generated contents from aesthetic and technical perspectives. In *Proceedings of the IEEE/CVF International Conference on Computer Vision*. 20144–20154.
- [46] Rongyuan Wu, Lingchen Sun, Zhiyuan Ma, and Lei Zhang. 2024. One-step effective diffusion network for real-world image super-resolution. *Advances in Neural Information Processing Systems* 37 (2024), 92529–92553.
- [47] Zeyu Xiao, Dachun Kai, Yueyi Zhang, Xiaoyan Sun, and Zhiwei Xiong. 2024. Asymmetric Event-Guided Video Super-Resolution. In *Proceedings of the 32nd ACM International Conference on Multimedia*. 2409–2418.
- [48] Zeyu Xiao, Zhiwei Xiong, Xueyang Fu, Dong Liu, and Zheng-Jun Zha. 2020. Space-time video super-resolution using temporal profiles. In *Proceedings of the 28th ACM International Conference on Multimedia*. 664–672.
- [49] Rui Xie, Yinhong Liu, Penghao Zhou, Chen Zhao, Jun Zhou, Kai Zhang, Zhenyu Zhang, Jian Yang, Zhenheng Yang, and Ying Tai. 2025. STAR: Spatial-Temporal Augmentation with Text-to-Video Models for Real-World Video Super-Resolution. *arXiv preprint arXiv:2501.02976* (2025).
- [50] Rui Xie, Chen Zhao, Kai Zhang, Zhenyu Zhang, Jun Zhou, Jian Yang, and Ying Tai. 2024. Addsr: Accelerating diffusion-based blind super-resolution with adversarial diffusion distillation. *arXiv preprint arXiv:2404.01717* (2024).
- [51] Binxin Yang, Shuyang Gu, Bo Zhang, Ting Zhang, Xuejin Chen, Xiaoyan Sun, Dong Chen, and Fang Wen. 2023. Paint by example: Exemplar-based image editing with diffusion models. In *Proceedings of the IEEE/CVF Conference on Computer Vision and Pattern Recognition*. 18381–18391.
- [52] Sidi Yang, Tianhe Wu, Shuwei Shi, Shanshan Lao, Yuan Gong, Mingdeng Cao, Jiahao Wang, and Yujiu Yang. 2022. Maniqa: Multi-dimension attention network for no-reference image quality assessment. In *Proceedings of the IEEE/CVF conference on computer vision and pattern recognition*. 1191–1200.
- [53] Xi Yang, Chenhang He, Jianqi Ma, and Lei Zhang. 2025. Motion-guided latent diffusion for temporally consistent real-world video super-resolution. In *European Conference on Computer Vision*. Springer, 224–242.
- [54] Peng Yi, Zhongyuan Wang, Kui Jiang, Junjun Jiang, Tao Lu, Xin Tian, and Jiayi Ma. 2021. Omniscient video super-resolution. In *Proceedings of the IEEE/CVF international conference on computer vision*. 4429–4438.
- [55] Peng Yi, Zhongyuan Wang, Kui Jiang, Junjun Jiang, and Jiayi Ma. 2019. Progressive fusion video super-resolution network via exploiting non-local spatio-temporal correlations. In *Proceedings of the IEEE/CVF international conference on computer vision*. 3106–3115.
- [56] Tianwei Yin, Michaël Gharbi, Richard Zhang, Eli Shechtman, Fredo Durand, William T Freeman, and Taesung Park. 2024. One-step diffusion with distribution matching distillation. In *Proceedings of the IEEE/CVF conference on computer vision and pattern recognition*. 6613–6623.
- [57] Fanghua Yu, Jinjin Gu, Zheyuan Li, Jinfan Hu, Xiangtao Kong, Xintao Wang, Jingwen He, Yu Qiao, and Chao Dong. 2024. Scaling up to excellence: Practicing model scaling for photo-realistic image restoration in the wild. In *Proceedings of the IEEE/CVF Conference on Computer Vision and Pattern Recognition*. 25669–25680.
- [58] Zongsheng Yue, Jianyi Wang, and Chen Change Loy. 2024. Resshift: Efficient diffusion model for image super-resolution by residual shifting. *Advances in Neural Information Processing Systems* 36 (2024).
- [59] Lvmin Zhang, Anyi Rao, and Maneesh Agrawala. 2023. Adding conditional control to text-to-image diffusion models. In *Proceedings of the IEEE/CVF International Conference on Computer Vision*. 3836–3847.
- [60] Yuehan Zhang and Angela Yao. 2024. Realviformer: Investigating attention for real-world video super-resolution. In *European Conference on Computer Vision*. Springer, 412–428.
- [61] Shangchen Zhou, Chongyi Li, Kelvin CK Chan, and Chen Change Loy. 2023. Propainter: Improving propagation and transformer for video inpainting. In *Proceedings of the IEEE/CVF international conference on computer vision*. 10477–10486.
- [62] Shangchen Zhou, Peiqing Yang, Jianyi Wang, Yihang Luo, and Chen Change Loy. 2024. Upscale-A-Video: Temporal-Consistent Diffusion Model for Real-World Video Super-Resolution. In *Proceedings of the IEEE/CVF Conference on Computer Vision and Pattern Recognition*. 2535–2545.